ADVANCED ENERGY MATERIALS
www.advenergymat.de

Ion Bridging by Carbon Dioxide Facilitates Electrochemical Energy Storage at Charged Carbon–Ionic–Liquid Interfaces

*Mingren Liu, Yong-Lei Wang, Konstantin Schutjajew, Liyuan Chai, and Martin Oschatz**

Solvent free ionic liquid (IL) electrolytes facilitate high-voltage supercapacitors with enhanced energy density, but their complex ion arrangement and through that the electrochemical properties, are limited by strong Coulombic ordering in the bulk state and like-charged ion repulsion at electrified interfaces. Herein, a unique interfacial phenomenon resulting from the presence of carbon dioxide loaded in 1-Ethyl-3-methylimidazoliumtetrafluorborate electrolyte that simultaneously couples to IL ions and nitrogen-doped carbonaceous electrode is reported. The adsorbed CO_2 molecule polarizes and mitigates the electrostatic repulsion among like-charged ions near the electrified interface, leading to an ion "bridge effect" with increased interfacial ionic density and significantly enhanced charge storage capability. The unpolarized CO_2 possessing a large quadrupole moment further reduces ion coupling, resulting in higher conductivity of the bulk IL and improved rate capability of the supercapacitor. This work demonstrates polarization-controlled like-charge attraction at IL–electrode–gas three-phase boundaries, providing insights into manipulating complex interfacial ion ordering with small polar molecule mediators.

1. Introduction

Adsorption of electrolyte ions at electrified interfaces is a fundamental electrochemical process of great importance.[1] In electric double layer capacitors (EDLCs), the charge storage capability primarily arises from capacitance generated through electrostatic interaction that leads to the formation of electric double layers (EDLs).[2] Solvent-based electrolytes usually form "compressed double-layers",[3] where the densification of counterions is mirrored by the accumulation of electrons or the formation of electron deficiencies in the solid electrodes, resulting in the ion layer thickening and shielding of the bulk electrolyte against the electrode potential.[4] This process is often accompanied by the distinct concentration gradients between solvated charge carriers, and the electrostatic interactions between ions are usually insignificant due to the screening effect of solvent molecules.[5]

Ionic liquids (ILs) are solvent-free electrolytes with a unique structure that has garnered significant interest in recent years.[6] Composed entirely of ions, IL electrolytes usually exhibit a larger electrochemical stability window than solvent-based electrolytes that promises to enhance the specific energy density of electrochemical energy storage devices.[6–7] Fundamentally, the presence of strong intermolecular forces and high space charge densities leads to a distinct EDL structure in ILs compared to those found in solvent-based systems.[8] The complex local structures and by that the physicochemical properties of ILs are primarily determined by a delicate balance of Coulombic interaction, hydrogen bonding, and other weak intermolecular forces.[9] Coulomb's law, which stipulates that opposite charges attract while like charges repel each other, governs the ionic ordering within the bulk liquid.[6,10] It has been estimated that the proportion of free ions in ILs is less than 15% at room temperature, resulting in low conductivity and high viscosity of this class of electrolytes.[11] More importantly, the complex intermolecular forces further generate the interfacial like-charge repulsion and charge oscillation, which principally limit the packing of counterions at electrified interfaces and thus, the capacitive performance of devices.[6,10a,12]

Recent studies on ILs functionalized with hydroxyl[10a,13] or amphiphilic groups[12b] have brought to light that the enhanced hydrogen bonds or van der Waal's interactions contribute to mitigating the electrostatic repulsion between like-charged cations.[14] By further lowering the attractive interaction with weakly coordinating anions, the formation of a cationic bilayer at the electrode interface becomes possible.[8b,10b] It is noted that

M. Liu, L. Chai
Institute of Environmental Science and Engineering, School of Metallurgy and Environment
Central South University
Changsha 410083, P. R. China
M. Liu, K. Schutjajew, M. Oschatz
Institute for Technical Chemistry and Environmental Chemistry
Center for Energy and Environmental Chemistry Jena (CEEC Jena)
Friedrich-Schiller-University Jena
Philosophenweg 7a, 07743 Jena, Germany
E-mail: martin.oschatz@uni-jena.de
Y.-L. Wang
Department of Materials and Environmental Chemistry
Arrhenius Laboratory
Stockholm University
Stockholm SE-106 91, Sweden

The ORCID identification number(s) for the author(s) of this article can be found under https://doi.org/10.1002/aenm.202300401

DOI: 10.1002/aenm.202300401

modifying anions with long neutral tails as surface-active IL electrolytes also results in unusual interfacial ion distributions, where at high temperatures over 130 °C, non-polar domains are formed with self-assembled large alkyl tails of anions.[12b] Excess cations are thus squeezed into the first layer, leading to alleviated like-charge repulsion at the electrified interface. Attempts to modify the electrode surface have been further made through sterically confining ions into ultra-micropores of 0.7 nm, achieving a so-called "non-Coulombic ordering".[6,15] The repulsive electrostatic interaction between like-charged ions is partially screened by the image charges induced in the carbon pore walls, leading to the formation of cation–cation/anion–anion pairs.[6] These discoveries have laid the foundation for manipulating interfacial like-charge attraction but integrating such artificially modified EDLs into practical application remains challenging. The difficult synthesis pathways, the high viscosity of modified ILs at room temperature, and the limited ionic diffusivity in narrow pores may all potentially impair practical performance of devices that promise outstanding rate capability during fast charge/discharge process.[16] To enhance the specific energy density without compromising the power density, an alternative strategy for modifying EDL structures is desired. This could involve the addition of a stable mediator that enhances interactions with the electrode surface and between the adsorbed IL ions. Intriguingly, small gas molecules may be promising additives to IL electrolytes, as bulk ILs, pore-confined ILs, and EDLs formed with solvent-based electrolytes can all create excellent environments for gas adsorption and respond to the presence of gases with changes in their local ionic structures.[17] Moreover, given the interfacial nano-structure where polar gas can interact with a heteroatom-doped electrode surface and electrolyte ions,[18] polarizable gas molecules present significant potential to form gas-IL pairs on the electrode/electrolyte interface and modulate the EDL structure for enhanced charge storage capabilities.[18b,19]

The high solubility and unique dissolution behavior of carbon dioxide (CO_2) in IL,[20] along with its large quadrupole moment to form CO_2-ion pairs and polarizability to form a dipole moment,[18a,21] make it a highly attractive additive for IL electrolytes. This has led to investigations into the effect of CO_2 loading in the 1-Ethyl-3-methylimidazoliumtetrafluorborate ($EMIMBF_4$) IL electrolyte coupled with nitrogen-free/doped carbon electrodes as a proof-of-concept. Results reveal that CO_2 strengthens the coupling between the IL ions and the nitrogen-doped charged electrode surface, leading to a phenomenon referred to as the "bridge-effect". Specifically, CO_2 molecules absorbed on the electrified electrode surface act as a mediator between like-charged cations, reducing their coulombic repulsion and allowing for a higher packing density in the first layer. This process is rationalized by the polarization of CO_2 with the frustrated $[EMIM]^+$-pyridinic-nitrogen couples under negative electrode charges. The large quadrupole moment of unpolarized CO_2 further alleviates the Coulombic ordering in the bulk IL. These effects lead to significantly enhanced capacitances and improved rate capabilities of symmetrical supercapacitors while maintaining the electrochemical stability of the IL electrolyte. This work provides insights into understanding and controlling the complex interfacial ionic structure through interplay between electrode surface, electrolyte ions, and polarizable gases.

2. Results and Discussion

2.1. Preparation and Structural Characterization of the Electrode Materials

Salt-templated carbon (STC) was synthesized by employing sucrose as the carbon precursor and $ZnCl_2$ as the porogen with a mass ratio of $ZnCl_2$ to sucrose of 8.[4] After polycondensation at 160 °C and subsequent carbonization at 900 °C, STC carbon with hierarchical pore structure was obtained. The corresponding nitrogen-doped STC (NDSTC) reference material was further prepared via a previously reported post-functionalization process with cyanamide at 800 °C.[4]

Transmission electron microscopy (TEM) was used to investigate the carbon nanostructures of STC and NDSTC. The TEM image (**Figure 1**a) reveals that the salt templating endows STC with open morphology and a structure including mesopores, which is preserved in NDSTC even after nitrogen doping (Figure 1b). This finding is consistent with previous studies[4,17a] and indicates that the nitrogen heteroatoms bonded to carbon network have no significant effect on the pore architecture. N_2 physisorption experiments (Figure 1c) further reveal that STC and NDSTC exhibit the typical type IV isotherms[22] with a hysteresis loop in the relative pressure range between 0.4 and 0.9, indicative of a mesopore-containing structure.[4] Both isotherms are nearly identical in shape and nitrogen uptake. The pore size distribution analysis (Figure 1d) based on the quenched-solid density functional theory (QSDFT) confirms mesopores in STC and NDSTC with sizes ranging from 2 to 7 nm. Comparable specific surface areas (SSAs) are further obtained for STC (2109 $m^2\ g^{-1}$) and NDSTC (2001 $m^2\ g^{-1}$), where the total pore volumes (V_t) of 1.40 $cm^3\ g^{-1}$ for STC and 1.30 $cm^3\ g^{-1}$ for NDSTC are also similar (Table S1). Both materials exhibit micropore volumes of 0.35 $cm^3\ g^{-1}$ and the cumulative pore size distribution plots for NDSTC (Figure 1e) show a slight decrease in the mesopore content larger than 5 nm, likely caused by the reheating procedure. In contrast to solvent-based electrolytes with unfavorable ion-solvent separation effect, this hierarchical porous structure in STC and NDSTC with dominant mesopores contributes to in-pore ion diffusion and thus favors the power demand for IL-based supercapacitors.

While the solubility of CO_2 in pristine IL generally decreases at elevated temperatures due to reduced adsorption energy, recent studies have highlighted the significant impacts of the confinement effect on the gas uptake capacities and kinetics in ILs.[17a,23] CO_2 physisorption measurements were thus conducted on both pristine IL and IL infiltrated in the pores of STC (IL@STC) and NDSTC (IL@NDSTC) (Figure S1, Supporting Information). The volumetric CO_2 sorption isotherms exhibit a maximum CO_2 uptake of 2.2 $cm^3\ g^{-1}$ in pristine IL at 293 K and 1 bar CO_2 pressure, which decreases to 1.8 $cm^3\ g^{-1}$ at 313 K. In contrast, significantly higher CO_2 uptake (normalized to the IL content) of 6.4 and 6.2 $cm^3\ g^{-1}$ were observed in IL@STC and IL@NDSTC at 293 K, respectively, along with a retention of relatively high CO_2 uptakes at 313 K (4.1 $cm^3\ g^{-1}$ for IL@STC and 5.5 $cm^3\ g^{-1}$ for IL@NDSTC). This finding suggests that nano-pore confinement promotes the formation of interionic voids for CO_2 embedding and enhances CO_2-ion interaction with higher CO_2 retention at elevated temperatures. The enhancement by nitrogen

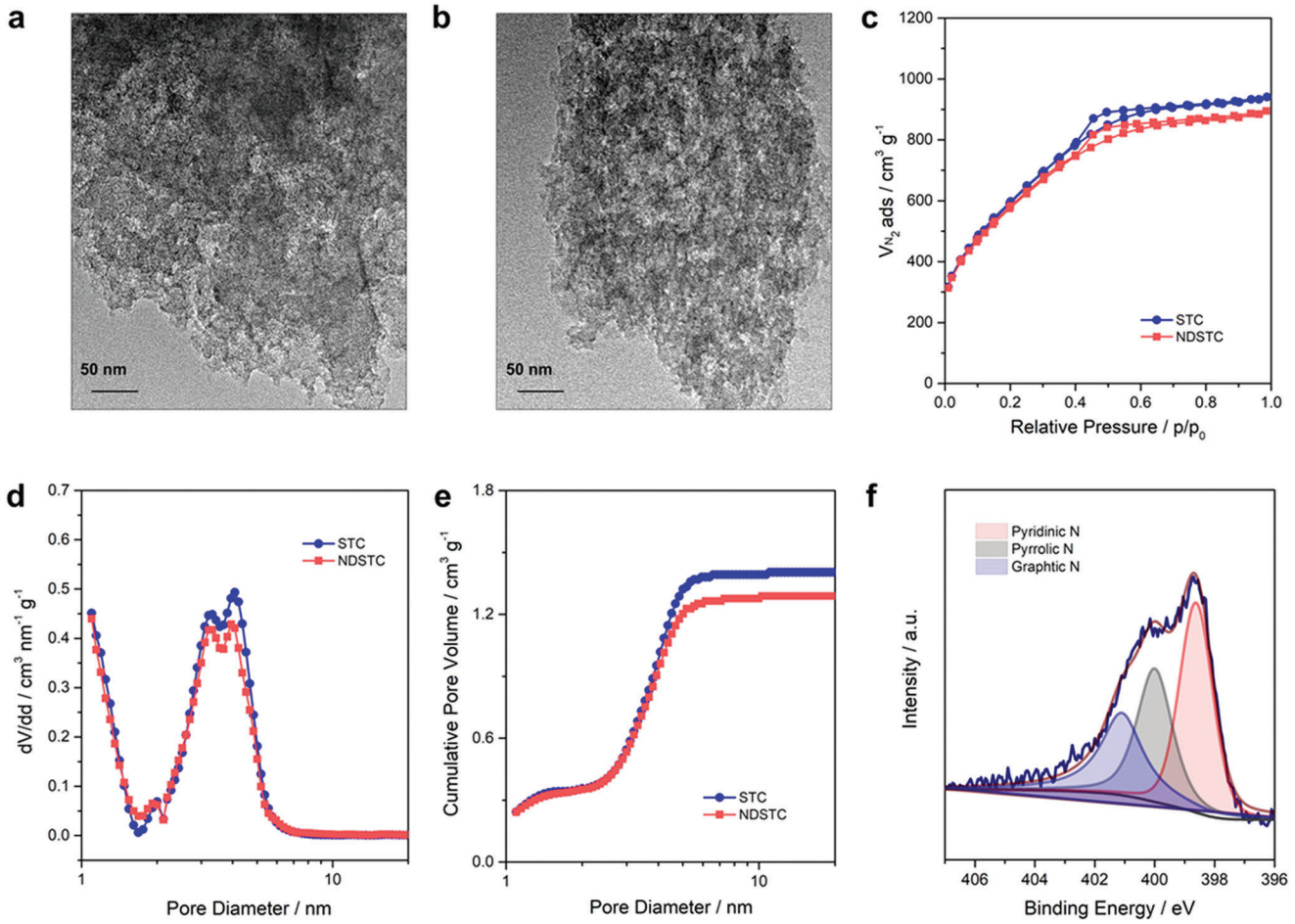

Figure 1. Characterization of STC and NDSTC: TEM images of a) STC and b) NDSTC; c) Nitrogen physisorption isotherms measured at 77 K; d) Differential plots of pore size distributions calculated from QSDFT model, adsorption branch kernel; e) Cumulative pore size distribution plots; f, Fitted high-resolution XPS N1s spectrum of NDSTC.

doping further suggests that the inhomogeneous electron density distribution within the carbon pore walls changes the structure of IL ions and the adsorption state of CO_2.[6,17a] The limited thermal expansion of IL in this NDSTC confinement thus preserves the structural integrity of ionic ordering at high temperature.[17a,24] This is also evidenced by the CO_2 physisorption measurements on the empty STC and NDSTC materials where a higher uptake is obtained for NDSTC despite of the slightly lower SSA (Figure S1c, Supporting Information).

Elemental analysis of NDSTC reveals a nitrogen content of 6.6 at.% (Table S1, Supporting Information), which is in accordance with the results obtained from X-ray photoelectron spectroscopy (XPS), showing a nitrogen content of 6.5 at.% (Figure S2a, Supporting Information). No significant content of nitrogen can be detected in STC but comparable oxygen contents were found in both materials (Tables S1 and S2, Supporting Information). Deconvolution of the high-resolution N1s spectrum of NDSTC (Figure 1f) into three peaks representing pyridinic nitrogen (398.5 eV), pyrrolic nitrogen (400.0 eV), and graphitic nitrogen (401.2 eV) indicates a high content of pyridinic nitrogen (40.1 at.%) among the overall doped nitrogen.[25] This finding is of particular significance, as basic pyridinic nitrogen containing lone electron pairs can not only promote interaction between electrode surface and ions, but also result in a particularly strong interaction with CO_2 loaded in ILs.[24,26] In the subsequent analysis, the electrochemical properties of these two model materials with nearly similar pore structure but different surface polarity will be compared with a special focus on the impact of CO_2 modification on the IL electrolyte and the formation of EDLs.

2.2. Electrochemical Characterization

The electrochemical performance of pure $EMIMBF_4$ IL and CO_2 loaded IL (IL+CO_2) electrolytes coupled with STC and NDSTC electrodes was first investigated in the symmetrical two-electrode device. The cyclic voltammograms (CVs, **Figure 2**a; Figure S3, Supporting Information) obtained from all samples exhibit a quasi-rectangular shape, as typically observed in IL-based supercapacitors.[16] Notably, the integral area increases by more than 35% in the device with NDSTC electrodes after the introduction of CO_2 while the shape of the CVs does not demonstrate a significant change. On the contrary, the comparative CV curves of the device with STC electrodes do not exhibit such a considerable enhancement in the integral area when

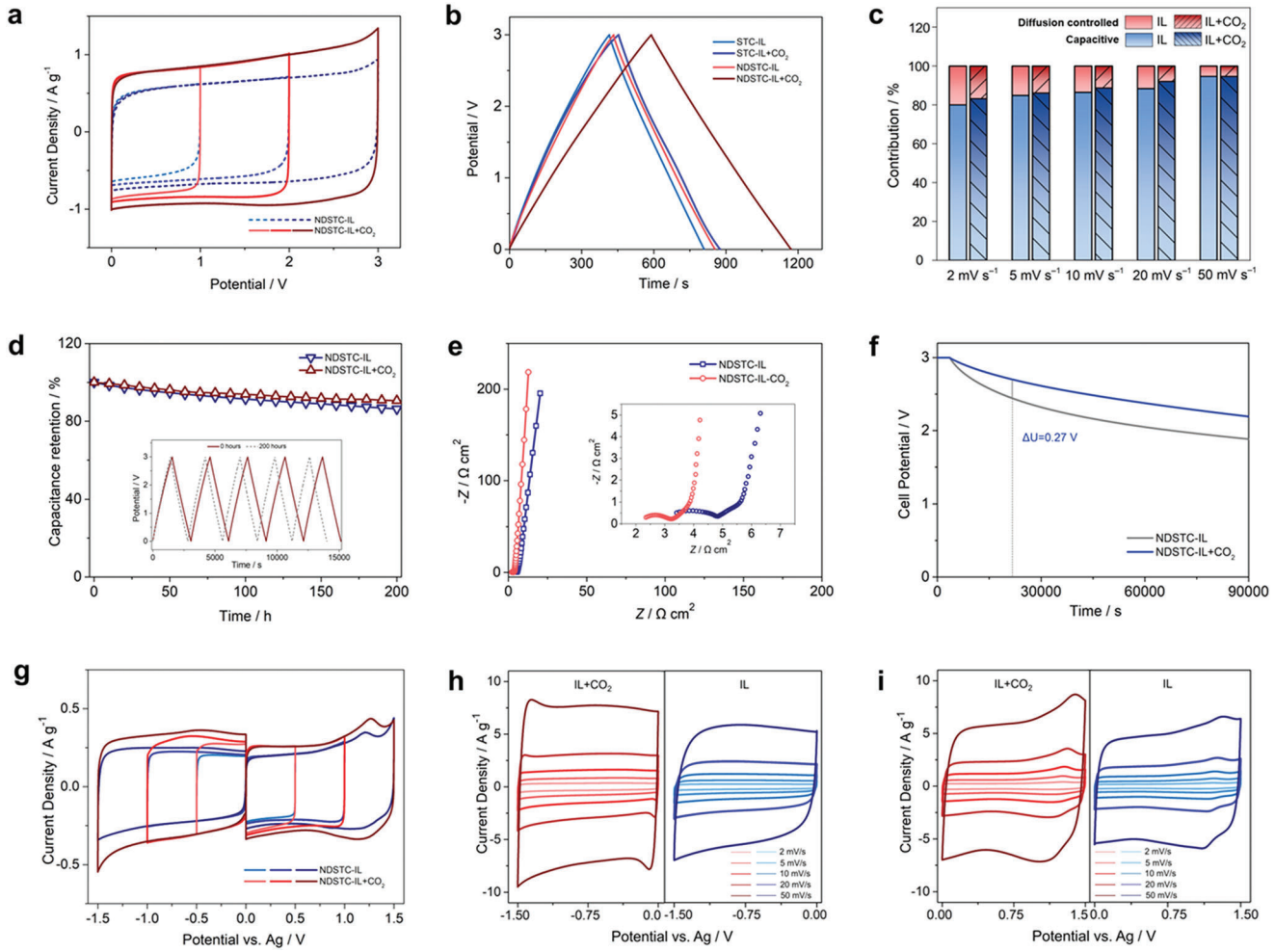

Figure 2. Electrochemical measurements with IL and IL+CO_2 electrolytes, a–f) Electrochemical measurements in symmetrical two-electrode supercapacitors: a) CV curves with NDSTC electrodes tested at 10 mV s^{-1}; b) GCPL profiles of two-electrode devices at 0.5 A g^{-1}; c) Capacitive and diffusion-controlled contribution in the two-electrode devices with NDSTC electrodes at different scan rates; d) Floating voltage test of NDSTC-IL+CO_2 device at a current density of 0.2 A g^{-1} for 200 h (insert is the five cycles of charge/discharge curves at 0 and 200 h); e) Nyquist plots of two-electrode NDSTC-IL and NDSTC-IL+CO_2 devices; f) Self-discharge test for the NDSTC-IL and NDSTC-IL+CO_2 devices at room temperature. g–i) Electrochemical measurements of half-cells in the three-electrode configuration with NDSTC electrode: g) three-electrode CV curves at 2 mV s^{-1}, and h-i) CV curves at different scan rates from 2 to 50 mV s^{-1} with negative electrode polarization (h) and positive electrode polarization (i).

CO_2 is present during cycling. Consistent with the rectangular shapes of the CVs, the galvanostatic charging/discharging with potential limitation (GCPL) profiles in Figure 2b and Figure S4 (Supporting Information) display the typical triangular shapes, with the specific capacitances in the order of NDSTC-IL+CO_2 > STC-IL+CO_2 > NDSTC-IL > STC-IL as 193, 147, 141, 132 F g^{-1} at 0.5 A g^{-1}, respectively. Moreover, a rate capability of 91.2% (176 F g^{-1}, Figure S5a, Supporting Information) and an IR drop of 0.042 V (Figure S4, Supporting Information) at 10 A g^{-1} is achieved on the NDSTC-IL+CO_2 electrode.

After balancing between the high-energy demand and the voltage stability for practical application, the voltage window of NDSTC-IL+CO_2 device is further expanding to 3.4 V (Figure S6, Supporting Information).[27] The GCPL profiles exhibit a comparable coulombic efficiency over 98.5% and a specific capacitance of 198 F g^{-1} at a low current density of 0.5 A g^{-1}, indicating that no significant side reactions are induced with higher voltages. Accordingly, the NDSTC-IL+CO_2 electrode delivers a specific energy of 63.4 Wh kg^{-1} at 75.6 W kg^{-1}, along with a power density of 7363 W kg^{-1} at 53.5 Wh kg^{-1} within a voltage window of 3.0 V (Figure S5b, Supporting Information). When the voltage is set to 3.4 V, specific energies of 86.1 Wh kg^{-1} at 81.2 W kg^{-1} and 69.0 Wh kg^{-1} at 8295 W kg^{-1} can be achieved on the NDSTC-IL+CO_2 electrode, suggesting an enhanced energy-power synergistic output ability (Figure S6d–f, Supporting Information). Further maximization of energy density from the device level is made possible with the comparable charge storage performance in the NDSTC-IL+CO_2 device with halved electrolyte dosage (Figure S7, Supporting Information). These observed differences in charge storage capability underscore the importance of both CO_2 addition and a more polar electrode surface. Given the orientation-rearrangement of interfacial counterions under electrode polarization, the enhanced performance of NDSTC-IL+CO_2 device suggests the existence of a special

interaction between CO_2 and both the interfacial electrolyte ions and nitrogen atoms on the electrode surface, which, in turn, seems to modify the formed EDL structure and allows for the higher charge storage capability.[6,12b,25,28]

To further decouple the interplay between surface adsorption and electron transfer process, capacitance differentiation analysis was conducted by separating the current response in the CV curves into capacitive and diffusion-controlled charge storage mechanisms using the equation:[29]

$$i(V) = k_1 v + k_2 v^{1/2} \quad (1)$$

where $k_1 v$ represents surface-reaction-dominant contribution as known from EDLCs, and $k_2 v^{1/2}$ corresponds to the diffusion-dominated contribution. Both the NDSTC-IL and NDSTC-IL+CO_2 devices exhibit a comparably large surface-dominant contribution of over 90% at 10 mV s^{-1} (Figure 2c; Figure S8, Supporting Information), indicating the continuing dominant role of the surface-adsorption process even after the addition of CO_2.[3,16] The long-term stability of the NDSTC-IL+CO_2 device was further evaluated with a floating voltage test (Figure 2d) that holds the device voltage at 3.0 V and room temperature for 200 h and interrupts the process by cycling at 0.2 A g^{-1} for six cycles every 10 h.[4] It's found that the NDSTC-IL+CO_2 device exhibits a higher capacitance retention of 90.6% compared to that of 85.7% in the NDSTC-IL device. The GCPL curves of the NDSTC-IL+CO_2 device show no significant increase in the internal resistance after 200 h with the remained triangular shape and the slightly increased IR drop by 0.008 V. The floating test at 60 °C for 100 h further exhibits a considerable capacitance retention of 83.4% by the NDSTC-IL+CO_2 device (Figure S9b, Supporting Information). The slightly enhanced capacitance retention of the NDSTC-IL+CO_2 device over the NDSTC-IL device is more significant under stressful conditions, as indicated by the higher retention difference of 4.9% at 0.2 A g^{-1} (Figure 2d) over that of 1.8% at 2.0 A g^{-1} (Figure S9a, Supporting Information). With elevated temperatures, the difference in retention increases to 5.8% (Figure S9b, Supporting Information). This suggests that the adsorbed CO_2 in the inner Helmholtz plane possibly reduces the accumulation of unavoidable trace water from the hydrophilic IL.[30] The inhibited hydrolysis of the acidic C2-H position in the $[EMIM]^+$ cation or the fluorinated $[BF_4]^-$ anion on the hydrophilic NDSTC interface thus contributes to reduced electrolyte decomposition and improved floating stability.[27] The cycling test of the NDSTC-IL+CO_2 device (Figure S9c–e, Supporting Information) performed at 10 A g^{-1} for 10 000 cycles ends with a capacitance retention over 93.2% and a coulombic efficiency close to 100%, which is higher than that of 89.4% observed for the NDSTC-IL device. This result highlights improved cycling stability with lower contact- and diffusion-resistance, and thus lower thermal stress in NDSTC-IL+CO_2 device during fast processes.[31] Taken together, rather than from the CO_2 reduction or other side-reactions in IL, the outperformance of the NDSTC-IL+CO_2 device is suggested to originate from the formation of an anomalous EDL structure caused by the delicate interactions among adsorbed CO_2, surficial nitrogen, and electrolyte ions, which further enables improved long-term stability.

It is widely acknowledged that the strong coulombic interactions in bulk IL lead to the formation of cation-anion coordination shells with strong intermolecular forces and high space charge densities.[6,32] With the addition of CO_2 molecules with a large quadrupole moment (13.4×10^{-40} C m^2),[33] however, interactions between CO_2 and cations and anions are additionally introduced.[34] Such special interaction induces ionic polarization with a local electric field that weakens the electrostatic forces between cations and anions, resulting in an enlarged fraction of free ions.[32,35] To investigate this possible mechanism, a comprehensive study was conducted using electrochemical impedance spectroscopy (EIS), ionic conductivity and viscosity tests, and galvanostatic intermittent titration technique (GITT). The Nyquist plots (Figure 2e) show a smaller intrinsic ohmic resistance R_s in the two-electrode NDSTC-IL+CO_2 device, suggesting enhanced ionic conductivity in the IL+CO_2 electrolyte.[36] The shorter 45° transition line and smaller diameter semicircle further indicate that CO_2 enhances the ionic mobility and facilitates faster in-pore diffusion by decreasing the co-ion access and thus the in-pore ion population.[15,25,37] Correspondingly, the ionic conductivity test (Figure S10a, Supporting Information) shows that the ionic conductivity of the IL-CO_2 electrolyte increases over a wide temperature range from 0 to 80 °C. At 20 °C, the ionic conductivity of IL+CO_2 electrolyte reaches 17.54 mS cm^{-1}, which is higher than that of 11.58 mS cm^{-1} in pure IL electrolyte. A lower viscosity of IL+CO_2 electrolyte at 20 °C of 9.84 mPa s^{-1} than that of 15.77 mPa s^{-1} in pure IL electrolyte is further obtained (Figure S10b, Supporting Information).

The in-pore ion diffusion with IL+CO_2 electrolyte was further evaluated with the GITT test. Consistent with the CV, GCPL, and EIS results, the GITT curves of the NDSTC-IL+CO_2 device (Figure S11a, Supporting Information) display higher charge storage capability, diminished internal resistance, and a reduced self-discharge rate compared to the NDSTC-IL device. The diffusion coefficient D_{ion} profile calculated from the charging process (Figure S11b, Supporting Information) conforms to the physical models of EDLC behavior in IL-based supercapacitors, where the increase in D_{ion} value at moderate cell potential region arises from the balance of the increased in-pore ion population and electrostatic interactions.[15,38] A consistently higher D_{ion} value in the NDSTC-IL+CO_2 device over the NDSTC-IL device is obtained throughout the entire cell potential range, indicating enhanced ion diffusivity after the introduction of CO_2.[38] Notably, a lower diffusivity enhancement of IL+CO_2 electrolyte over pure IL electrolyte is observed during the discharging process (Figure S11c, Supporting Information), in consistency with the result from the self-discharge test (Figure 2f).[39] Typically, an electrolyte with reduced viscosity and heightened conductivity facilitates charge redistribution on the electrode surface and the diffusion of counterions away from EDLs, leading to an elevated self-discharge rate.[40] Nonetheless, a lower self-discharge rate in the NDSTC-IL+CO_2 device over the NDSTC-IL device is observed, where a less significant charge redistribution process in the first 6 h is obtained with a difference in OCV of 0.27 V. This result suggests that the NDSTC-IL+CO_2 device features both higher ion mobility in bulk electrolyte and an unusual EDL structure with enhanced ion coupling at electrified interface after the introduction of CO_2.[40]

The adsorption of CO_2 on the nitrogen-doped carbon surface is reported to be strengthened with external negative charges, resulting in charge redistribution within the adsorbed CO_2.[18a,41]

In this context, the specific influence of CO_2 on the negative and positive electrode, coupled with the distinct properties of cations and anions have been investigated in three-electrode half-cells (Figure 2g–i; Figure S12, Supporting Information). The CV curves of the NDSTC-IL+CO_2 half-cell in Figure 2g exhibit anomalous current polarity switching at the negative vertex potentials. Compared to the NDSTC-IL half-cell, the corresponding integral area with negative electrode polarization increases by ≈44% at 2 mV s^{-1}, suggesting the strong effect of present CO_2 on the adsorption state of cations.[28–29] Given the negative-charge-modulated polarization of CO_2 on nitrogen-doped carbon, it is hypothesized that adsorbed CO_2 molecules render like-charged cations closer to each other and lead to a denser packing on the IL–carbon interface. The integral areas in the CVs with positive electrode polarization and IL+CO_2 electrolyte increase by ≈23%, indicating that the CO_2 also enhances anionic packing but the observed effect of CO_2 on the free energy of adsorption of IL ions is more pronounced for cations.[28] The current versus sweep rate dependence ($i \approx \nu^{0.96}$) for negative electrode curves indicates an ideal shape with no mass transport limitation from 2 to 50 mV s^{-1} (Figure 2h; Figure S8d, Supporting Information).[7,42] The slight increase in current observed at around −0.05/−1.45 V versus Ag (Figure 2h) can be attributed to the spontaneous chemisorption/polarization and subsequent desorption/depolarization process of CO_2 molecules, which increases with rising scan rates.[43] Additionally, the current increase at +1.3 V versus Ag (Figure 2i) results from the size-matching effect of spherical-like anions and micropores with enhanced ion-pore interactions at high voltages.[44] Based on the three-electrode half-cell results, asymmetrical two-electrode devices with NDSTC as the negative electrode and STC as the positive electrode were assembled after charge balancing. Contrary CV responses were observed in IL and IL+CO_2 electrolytes when the electrode polarity was reversed (Figure S13, Supporting Information). The asymmetrical two-electrode device with IL electrolyte exhibits a slight increase (6.2%) in the integrated area of CV curves after reversing the electrode polarity, which may be attributed to the enhanced π–π interactions between the negative STC electrode and imidazole ring of the cation, as well as the higher anionic packing density on the positive NDSTC electrode.[15] In contrast, the integrated area in the asymmetrical device using IL+CO_2 electrolyte decreases significantly (15.1%) after reversing the electrode polarity to a negative STC electrode and positive NDSTC electrode. Along with the larger integrated areas for IL+CO_2-based device over IL-based device during negative scans, these findings suggest an enhanced ion-coupling effect at the electrified interface upon the addition of CO_2 and further emphasize the contribution of CO_2-ion pairs to charge storage on the negative NDSTC electrode.

In conclusion, the addition of CO_2 not only enhances the ion mobility in the bulk IL electrolyte with improved ionic conductivity and diffusivity, but also forms an anomalous EDL structure on the electrified NDSTC electrode surface that counteracts strong intermolecular Coulombic repulsion.[8a] Considering that the NDSTC electrode with high pyridinic-nitrogen content and rational pore structure favors ion adsorption and diffusion, the resulting stronger interfacial ion coupling further reduces the unfavorable "ion depletion effect" caused by the enhanced ionophilicity with nitrogen doping, and overcomes the cationic density limitation in the inner Helmholtz plane.[45] The inhibited self-discharge and significantly improved charge storage capability are thus obtained.[6] The adsorbed CO_2 also contributes to improving the long-term stability of the NDSTC-IL+CO_2 device.

2.3. Elucidation of Anomalous EDL Structures in NDSTC-IL+CO_2 Device

The EDL structures of the nano-cell models of STC-IL+CO_2, NDSTC-IL, and NDSTC-IL+CO_2 devices were analyzed using all-atomistic molecular dynamics (AAMD) simulation (**Figure 3**; Figure S14, Supporting Information). The number density (ρ_N) profiles of cations, anions, and CO_2 molecules are determined as a function of the distance from the electrode at varying potential differences. The result shows that counter-ions accumulate with strong ionic layering near the electrified interfaces, where the first- and second-neighbour scattering mainly contributes to the charge storage in EDLs.[6,46] At a potential difference of 3.0 V (Figure 3f,h), a denser cationic packing is observed in the NDSTC-IL+CO_2 nano-cell at ≈2.5 Å, accompanied by the accumulation of CO_2 on the negatively charged NDSTC surface and leading to a larger population of cations in the first layer. A sharp peak of CO_2 adsorption is observed at a similar distance (Figure 3h; Figure S15, Supporting Information). The accommodation of CO_2 results in the reorganization of neutral tails in the interfacial cations.[5a,47] Compared to the peaks of the secondary layer in STC-IL+CO_2 and NDSTC-IL nano-cells, the cationic ρ_N profile in NDSTC-IL+CO_2 nano cell at ≈5 Å appears as a shift of ≈1-Å-wide domain and a decrease in population (Figure 3f). Given the dominant role of first-two-layer ordering in determining the capacitance,[8c,46] this phenomenon indicates a more sufficient screening effect of electrode charges via excess cations in the first layer of NDSTC-IL+CO_2 nano cell, leading to higher interfacial charge carrier density, thinner EDL, and thus larger capacitance.[8b,35,48]

In the high voltage regime, $[EMIM]^+$ cations tend to align along the surface normally. The comparable densities observed in STC-IL+CO_2 and NDSTC-IL nano-cells suggest the packing density of cations in the first layer is limited (Figure 3f).[5a,10a,49] Using point charges and a dielectric constant of 12.0,[50] the simple coulombic interaction analysis estimates the repulsive energy between two cations at 5-Å-distance to be ≈12.0 kJ mol^{-1}.[6] Therefore, the excess oriented cations observed in NDSTC-IL+CO_2 nano-cell arise from an intermolecular mechanism that reduces the Coulombic repulsion and brings cations closer to each other.[6,12a] Note that surfacial nitrogen with extra electrons from electrode polarization promotes charge redistribution and further polarization of adsorbed CO_2 molecules.[18a] The screening effect of CO_2 molecules thus overcomes the strong repulsion between like-charged cations, leading to cation–cation rearrangement and densification.[6,9,13] The role of polarized CO_2 is termed as the ion "bridge effect" connecting IL ions and electrified electrode surface. Compared to the cationic ordering with successive multiple layers, a more concentrated layer structure of anions is indicated by a sharp peak at ≈3.0 Å (Figure 3g). $[BF_4]^-$ anions with a sphere-like shape and smaller size form a distinct EDL structure compared to $[EMIM]^+$ cations. This is also reflected

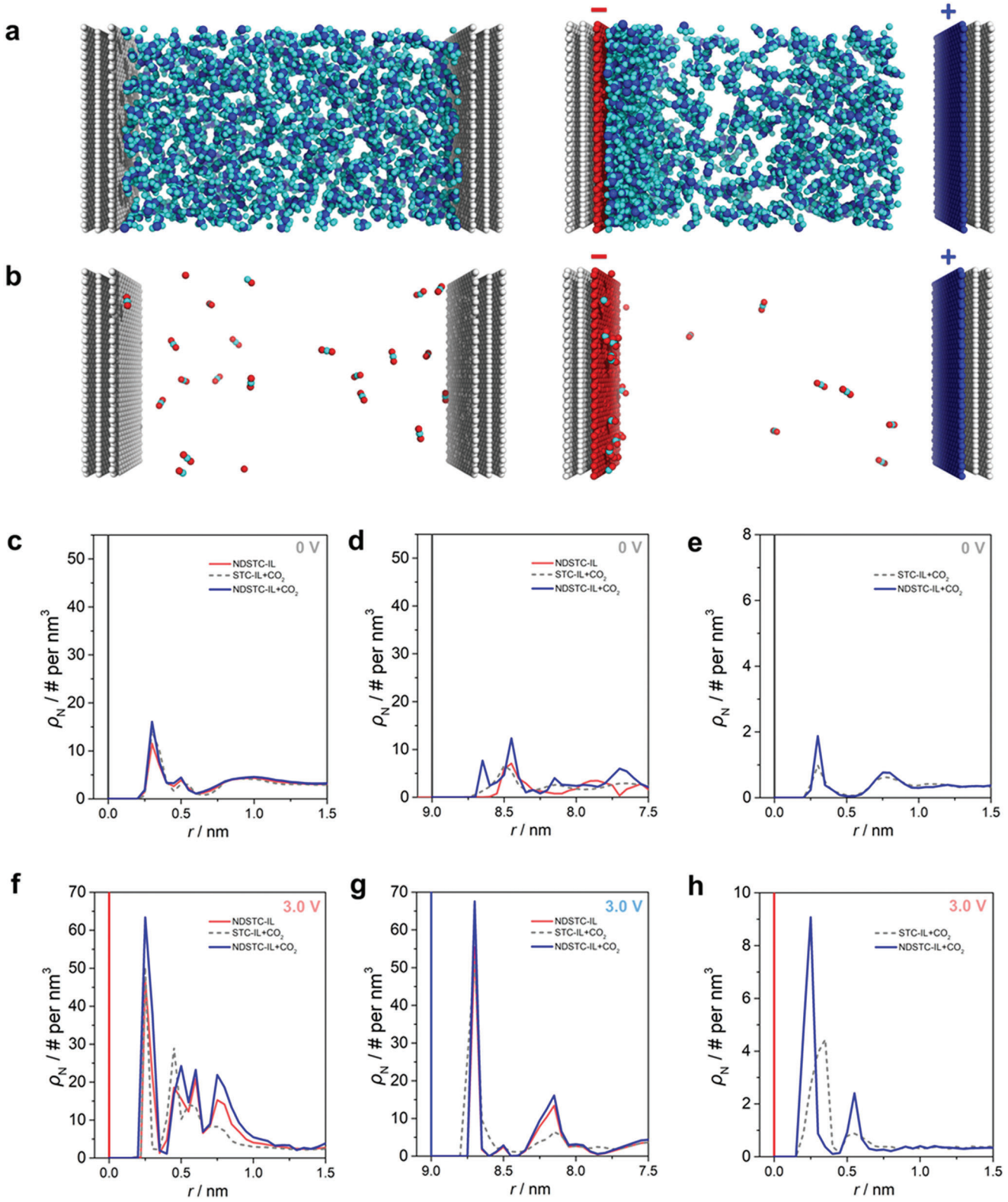

Figure 3. Molecular dynamics simulations of EDL structures in the nano-cell models: Snapshots of a) cations and b) CO_2 molecules at potential differences of 0 V (left panel) and 3.0 V (right panel) in the NDSTC-IL+CO_2 nano-cell; c–h) Number density distribution (ρ_N) of (c,f) cations, (d,g) anions, and (e,h) CO_2 molecules at potential differences of 0 V (Top) and 3.0 V (Bottom) in the NDSTC-IL, STC-IL+CO_2, and NDSTC-IL+CO_2 nano cells.

by the relatively high anionic densities in the first layer of STC-IL+CO_2 and NDSTC-IL nano cells.[6,8a] The broader peak of the STC-IL+CO_2 nano-cell further reveals the role of polar nitrogen-doped carbon surface in interacting with fluorine atoms and thus contributing to anionic packing.[15] Due to the reduced ion coupling in the presence of CO_2 and the coordination interactions between anions and CO_2, the anion-anion packing is enhanced with denser anion density in the NDSTC-IL+CO_2 nano-cell (Figure 3g).[6,12b]

To further elucidate the specific interaction site of CO_2 in the proposed "bridge effect", probability distribution analysis of CO_2 adsorbed on the ion-accumulated and electrified electrode surface was conducted.[51] The number density distribution suggests a preferential migration of CO_2 molecules to the negatively charged surface. A corresponding and relatively random distribution of adsorbed CO_2 on the STC electrode surface is observed (**Figure 4**a), even when the potential difference changes from 0 V to 3.0 V. In comparison, a more specific distribution of adsorbed CO_2 with areas of highest and lowest probabilities for cluster formation is observed on the negatively charged nitrogen-doped surface (Figure 4b).[6,51] The interaction probabilities between CO_2 and surfacial atoms at different potential differences are further quantified and normalized to the atomic contents determined from the XPS test. The normalized interaction probability distribution (Figure 4c) at 0 V is almost quartered regarding the surfacial carbon, pyridinic nitrogen, pyrrolic nitrogen, and graphitic nitrogen atoms, exhibiting less significant discrepancy in atomic affinity to CO_2. This result differs from the gas adsorption on single solid/gas interfaces that considers uncharged pyridinic nitrogen as the main active site.[24,52] With the increased potential differences, the interaction probability between CO_2 and pyridinic nitrogen on the negatively charged surface is steadily increasing from 26.2% at 0 V to 48.1% at 3.0 V, whereas that of surficial carbon atoms exhibits the corresponding decrease. The interaction probabilities between pyrrolic nitrogen, graphitic nitrogen, and CO_2 show less dependence on the electrode polarization. Given the high ionic concentration and space charge densities of IL electrolyte, the importance of electrode polarization is thus highlighted in the IL–electrode–gas three-phase boundaries, leading to the adsorption of CO_2 molecules on the electrified pyridinic-nitrogen sites with enhanced interaction (Figure 4d).[24,26]

Nuclear magnetic resonance (NMR) spectra are collected to identify the intermolecular charge redistribution caused by the bridge effect. Four systems were studied, including pure IL, IL with CO_2, IL with additional pyridine to represent the pyridinic-nitrogen doping, and IL with both CO_2 and pyridine. The variations of the chemical shift are in good consistency: the peak at around 9.0 ppm in ^{1}H NMR spectra (Figure 4e) has a slight downshift of −0.08 ppm in the IL+Pyridine+CO_2 sample compared to that in the pure IL, indicating the weakened cation-anion electrostatic interaction and thus increased shielding effect on the C(2)-H atom of imidazolium ring.[18b,53] Correspondingly, in the 2D ^{1}H-^{15}N heteronuclear multiple bond correlation (HMBC) spectra (Figure 4g), the peaks of N1-H2 correlations also show a downshift from δN/δH = 171.05/9.02 ppm in pure IL to δN/δH = 170.62/8.94 ppm in IL+Pyridine+CO_2 sample due to the mediator effect of CO_2 to the anions. The peaks of pyridinic N-H(A) correlations at δN/δH = 66.46/8.54 ppm in IL+Pyridine sample further exhibit a slight upfield shift to δN/δH = 66.06/8.52 ppm in IL+Pyridine+CO_2 sample, which could be ascribed to an increase of electron density in the surroundings after coordinating with CO_2. The asymmetrical peaks of ^{19}F NMR spectra (Figure 4f) with an upfield shift of −0.41 ppm from pure IL to IL+Pyridine+CO_2 sample indicate CO_2 also increases the charge density around F atoms.[18b] Thus, the spontaneous interaction between CO_2, pyridinic nitrogen and C(2)-H in cation, and the association between CO_2 and anion are confirmed. It's worth mentioning that in a practical device, the electrical polarization and the enrichment of CO_2 with pore confinement could further promote such charge redistribution.[18b] A profound polarization process of CO_2 on the negatively electrified NDSTC surface is thus deduced.[18a,41] The pyrinidic nitrogen is nucleophilic with lone pair electrons while $[EMIM]^+$ behaves as electrophile via the C(2)-H.[54] The steric hindrance analogical to weak frustrated Lewis pairs thus creates an active region for the adsorbed CO_2.[37,52a,55] The electron-delocalized pyridinic nitrogen triggers the charge redistribution in CO_2 and the increased electron density in CO_2 oxygen atoms further induces hydrogen-bonding-like interactions with the C(2)-H.[55] The bonding and antibonding orbitals of adsorbed CO_2 thus interact with the unoccupied orbitals of electrophile and non-bonding orbitals of the nucleophile, respectively, leading to the polarization of CO_2 molecules.

To fully elucidate the local nanostructure of the "bridge-effect", angular distributions of first-neighbored cations and CO_2 molecules were further calculated. Both tilt (θ, between the pseudo-C_2 axis of imidazolium ring and the surface normal, Figure 4h) and twist (φ, between the methyl and the surface normal, Figure 4i) angles are introduced for the cationic orientation, while the tilt angle ω (between the C–O bonding and the surface normal) represents the orientation of the polarized CO_2 molecule (Figure 4j).[12a,56] With the increasing negative electrode polarization, a tilt angle θ of ≈94.5° at a potential difference of 3.0 V has the imidazolium ring almost perpendicular to the surface plane. A twist angle φ from ≈90° at 0 V to ≈0°/180° at 3.0 V further suggests the overturn of cations with ethyl groups repelled and methyl groups attracted, both contributing to further accommodation of interfacial cations. Accordingly, CO_2 molecules display a simultaneous coordination tendency with surficial nitrogen and imidazolium rings, resulting in a tilt angle ω of ≈60° at 3.0 V.

Figure 5 presents the comprehensive scenario in the NDSTC-IL+CO_2 supercapacitor. In the bulk IL (Process **II**), CO_2 with a large quadrupolar moment coordinates simultaneously with cations and anions, weakening the Coulombic ordering and thus facilitating the transport of free ions for enhanced ionic conductivity and mobility.[8a] On the positively charged nitrogen-doped electrode surface (Process **III**), the coordination interaction between anions and CO_2 molecules facilitates anionic packing into a denser first layer. In the inner Helmholtz plane with negative charges (Process **I**), the dipole of polarized CO_2 tends to align along the surface normally and the molecular plane of the C–O bond tilts up.[18a,41] The polarized CO_2 molecule acts as a bridge to connect the like-charged cations by specifically binding to the C(2)-H of cations. With partially screened Coulombic repulsion, the decreased equivalent distance between cations is obtained, leading to densified cationic packing.[6,10b,57] Surficial pyridinic nitrogen with external negative charges not only triggers charge redistribution in the adsorbed CO_2, but also anchors ion-CO_2 clusters closer to the electrode surface with higher

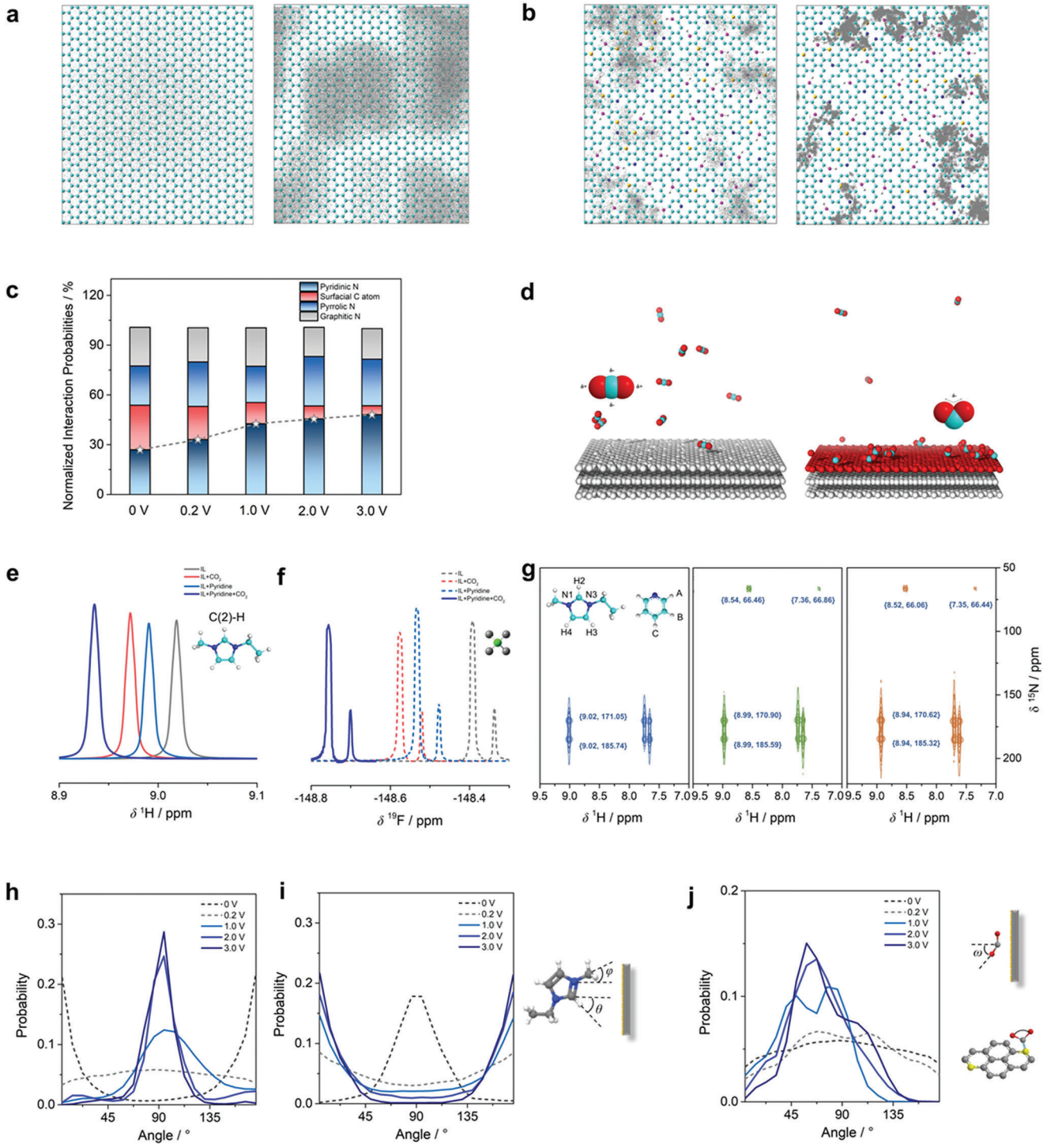

Figure 4. CO_2 orientation distributions and coordination with electrode and electrolyte ions: a,b) Probability distribution of CO_2 adsorption on STC electrode (a) and NDSTC electrode (b) at potential differences of 0 V (left panel) and 3.0 V (right panel); c) Normalized interaction probabilities between adsorbed CO_2 and surficial electrode atoms under negative electrode polarization of different potential differences; d) Snapshots of CO_2 adsorbed on negatively charged NDSTC electrode surface with potential differences of 0 V (left panel) and 3.0 V (right panel); e–g) ^{1}H (e) and ^{19}F (f) NMR spectra of ionic liquid with different additives; g) 2D ^{1}H-^{15}N HMBC NMR spectra of pure IL (left panel), IL+Pyridine sample (middle) and IL+Pyridine+CO_2 sample (right panel); h,i) Angular distributions of the imidazolium rings (θ, h) and methyl groups (φ, i) of $[EMIM]^{+}$ cations in the first layer under negative electrode polarization of different potential differences; j) Angular distributions of CO_2 (ω) located on the nitrogen-doped negatively charged electrode surface.

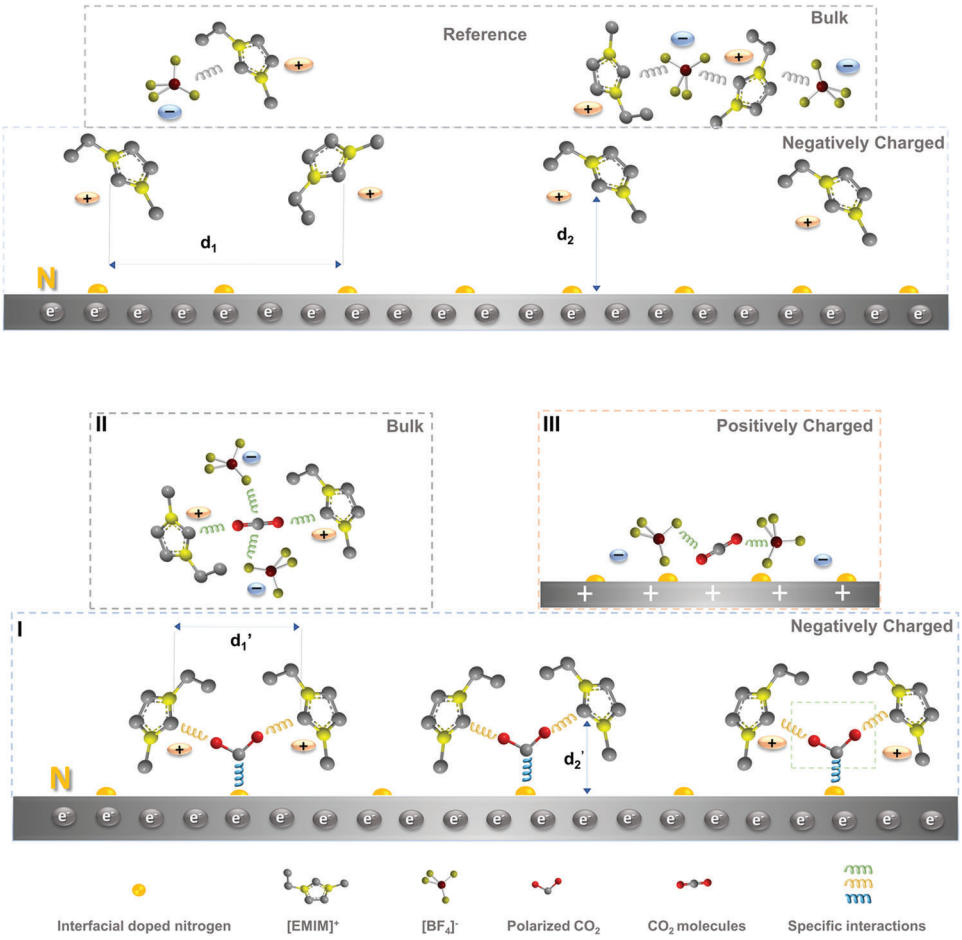

Figure 5. Schematic illustration of the proposed bridge effect of CO_2 on the IL structures (bottom) and the reference case without CO_2 (top) on the electrified nitrogen-doped electrode surface: Process **I** refers to polarized CO_2 molecules and their interaction with cations at the C(2)-H position and pyridinic nitrogen on the negatively charged electrode surface; d_1 and d_1'refer to equivalent distance between the electric centers of cations and d_2 and d_2' refer to equivalent distance between the nearest electric center of cations and electrode surface in NDSTC-IL and NDSTC-IL+CO_2 device, respectively; Process **II** refers to alleviated Coulombic ordering with CO_2 in the bulk IL; Process **III** refers to the coordination interaction between anion and CO_2 under positive electrode polarization.

charge storage capability and lower self-discharge rate.[12a,18a] This bridge effect breaks the density limitation of cations in the first layer, creating a delicate mixture of electrostatic-, dipole–dipole, and hydrogen-bonding interactions at the IL–electrode–gas three-phase boundaries.[10a,12b,13]

The present mechanisms are further applicable to diverse IL electrolytes where three ILs including 1-Ethyl-3-methylimidazolium bis(trifluoromethyls ulfonyl) imide (EMIMTFSI), 1-Butyl-3-methylimidazolium tetrafluoroborate ($BMIMBF_4$) and protic 1-butyl-1-methylpyrrolidinum bis(trifluoromethylsulfonyl)imide ($PyrH_4TFSI$) are selected (Figure S16, Supporting Information). It's noted that similar structural properties of cations with acidic Hydrogen-2 ($[EMIM]^+$ and $[BMIM]^+$) or protic Hydrogen-4 ($[PyrH_4]^+$) positions are shared in these ILs, whereas the $[TFSI]^-$ and $[BF_4]^-$ anions feature differences in electron density contrast and ion sizes. The as-assembled symmetrical two-electrode supercapacitors with these ILs and their CO_2-loaded counterparts along with NDSTC electrode all exhibit larger capacitances with enhancement ranging from 34% to 48% after the introduction of CO_2 (Figure S16, Supporting Information). These experimental findings corroborate the general applicability of the "bridge effect" as an intermolecular softening strategy for like-charge attraction.[5b,6]

Drawing on the Bazant–Storey–Kornyshev (BSK) theory and recent advancements in short-range and long-range screening, the decreased equivalent size of ions conduces to the short-range electrostatic force between the charged electrode and CO_2-ion clusters.[32,35,49,57] The CO_2 modification strategy, with its specific adsorption sites, offers a promising route toward improved energy storage performance in IL-supercapacitors. Although the current NDSTC-IL+CO_2 device does not outperform state-of-the-art IL-based supercapacitors,[15–16,40a,58] it paves the way for an energy storage concept with general applicability and fundamental improvements in charge storage capability, rate performance, and long-term stability of leading devices. Future work can focus on optimizing material structures, electrode manufacturing, electrolyte purification, and temperature dependency. It is also

noted that, due to their solubility and state, CO_2 molecules may effectively modify the EDL structures in neutral and alkali aqueous electrolytes.[17b] Exploring other gases, such as H_2S and SO_2, could guide future endeavors aimed at further investigating the IL-electrode-gas three-phase boundaries.

3. Conclusion

An interfacial phenomenon has been demonstrated in which CO_2 loaded in the IL electrolyte induces an intermolecular screening effect and facilitates charge storage on the nitrogen-doped electrode surface. Through systematic electrochemical investigations and AAMD simulations, the observed "bridge effect" is elaborated as pyridinic nitrogen groups form polarization couples with the imidazolium rings of $[EMIM]^+$ cations and trigger the polarization of adsorbed CO_2. The polarized CO_2 acts as mediators to reduce like-charge repulsion between interfacial cations, leading to stronger ion coupling and denser ion packing in the first layer. This ion-bridging technique effectively overcomes the density limitation of interfacial ions, contributing to a remarkable 44% increase in specific capacitance in a three-electrode half-cell with negative electrode polarization and an overall 35% increase in specific capacitance in a symmetrical supercapacitor with enhanced electrochemical stability. Additionally, the large quadrupole moment of unpolarized CO_2 weakens the Coulombic ordering, leading to higher ionic conductivity and diffusivity of the bulk IL, and better rate capability of the supercapacitors. This CO_2-modification strategy lays the foundation for future exploration of small polar additives to optimize the interfacial nanostructures in IL-based supercapacitors, and more broadly, provides a binary perspective for the distinct double-layer theories concerning solvent- and non-solvent-based systems.

Supporting Information

Supporting Information is available from the Wiley Online Library or from the author.

Acknowledgements

M.L. acknowledges financial support from China Scholarship Council (CSC). All authors thank Dr. Antje Völkel from Max Planck Institute of Colloids and Interfaces for providing the elemental analysis data and Dr. Timo Stettner from Friedrich-Schiller-University Jena, group of Prof. Dr. Andrea Balducci, for providing the protic ionic liquid. The computations were enabled by resources provided by Swedish National Infrastructure for Computing (SNIC) at PDC, HPC2N, and NSC partially funded by Swedish Research Council through grant agreement no. 2016–07213.

Open access funding enabled and organized by Projekt DEAL.

Conflict of Interest

The authors declare no conflict of interest.

Data Availability Statement

The data that support the findings of this study are available from the corresponding author upon reasonable request.

Keywords

carbon dioxide, electrode/electrolyte interface, ionic liquids, like-charge attraction, molecular dynamics simulations, supercapacitors

Received: February 7, 2023
Revised: March 20, 2023
Published online: April 20, 2023

[1] P. Srimuk, X. Su, J. Yoon, D. Aurbach, V. Presser, *Nat. Rev. Mater.* **2020**, *5*, 517.
[2] H. Shao, Y. C. Wu, Z. Lin, P. L. Taberna, P. Simon, *Chem. Soc. Rev.* **2020**, *49*, 3005.
[3] P. Zhang, M. Wang, Y. Liu, S. Yang, F. Wang, Y. Li, G. Chen, Z. Li, G. Wang, M. Zhu, R. Dong, M. Yu, O. G. Schmidt, X. Feng, *J. Am. Chem. Soc.* **2021**, *143*, 10168.
[4] R. Yan, M. Antonietti, M. Oschatz, *Adv. Energy Mater.* **2018**, *8*, 1800026.
[5] a) Y. Wu, J. Ye, G. Jiang, K. Ni, N. Shu, P. L. Taberna, Y. Zhu, P. Simon, *Angew. Chem., Int. Ed.* **2021**, *60*, 13317; b) P. Simon, Y. Gogotsi, *Nat. Mater.* **2020**, *19*, 1151; c) Q. Dou, S. Lei, D. Wang, Q. Zhang, D. Xiao, H. Guo, A. Wang, H. Yang, Y. Li, S. Shi, X. Yan, *Energy Environ. Sci.* **2018**, *11*, 3212.
[6] R. Futamura, T. Iiyama, Y. Takasaki, Y. Gogotsi, M. J. Biggs, M. Salanne, J. Segalini, P. Simon, K. Kaneko, *Nat. Mater.* **2017**, *16*, 1225.
[7] Y. Li, H. Shao, Z. Lin, J. Lu, L. Liu, B. Duployer, P. O. A. Persson, P. Eklund, L. Hultman, M. Li, K. Chen, X. Zha, S. Du, P. Rozier, Z. Chai, E. Raymundo-Pinero, P. L. Taberna, P. Simon, Q. Huang, *Nat. Mater.* **2020**, *19*, 894.
[8] a) M. V. Fedorov, A. A. Kornyshev, *Chem. Rev.* **2014**, *114*, 2978; b) M. Z. Bazant, B. D. Storey, A. A. Kornyshev, *Phys. Rev. Lett.* **2011**, *106*, 046102; c) S. Baldelli, *J. Phys. Chem. Lett.* **2013**, *4*, 244.
[9] D. H. Zaitsau, V. N. Emel'yanenko, P. Stange, S. P. Verevkin, R. Ludwig, *Angew. Chem., Int. Ed.* **2019**, *58*, 8589.
[10] a) A. Strate, T. Niemann, D. Michalik, R. Ludwig, *Angew. Chem., Int. Ed.* **2017**, *56*, 496; b) T. Niemann, A. Strate, R. Ludwig, H. J. Zeng, F. S. Menges, M. A. Johnson, *Angew. Chem., Int. Ed.* **2018**, *57*, 15364.
[11] G. Feng, M. Chen, S. Bi, Z. A. H. Goodwin, E. B. Postnikov, N. Brilliantov, M. Urbakh, A. A. Kornyshev, *Phys. Rev. X* **2019**, *9*, 021024.
[12] a) S. Bi, H. Banda, M. Chen, L. Niu, M. Chen, T. Wu, J. Wang, R. Wang, J. Feng, T. Chen, M. Dinca, A. A. Kornyshev, G. Feng, *Nat. Mater.* **2020**, *19*, 552; b) X. Mao, P. Brown, C. Cervinka, G. Hazell, H. Li, Y. Ren, D. Chen, R. Atkin, J. Eastoe, I. Grillo, A. A. H. Padua, M. F. Costa Gomes, T. A. Hatton, *Nat. Mater.* **2019**, *18*, 1350; c) C. Merlet, B. Rotenberg, P. A. Madden, P. L. Taberna, P. Simon, Y. Gogotsi, M. Salanne, *Nat. Mater.* **2012**, *11*, 306; d) S. Zhang, J. Zhang, Y. Zhang, Y. Deng, *Chem. Rev.* **2017**, *117*, 6755.
[13] T. Niemann, H. Li, G. G. Warr, R. Ludwig, R. Atkin, *J. Phys. Chem. Lett.* **2019**, *10*, 7368.
[14] A. Knorr, R. Ludwig, *Sci. Rep.* **2015**, *5*, 17505.
[15] X. Wang, M. Salari, D. Jiang, J. C. Varela, B. Anasori, D. J. Wesolowski, S. Dai, M. W. Grinstaff, Y. Gogotsi, *Nat. Rev. Mater.* **2020**, *5*, 787.
[16] Z. Li, S. Gadipelli, H. Li, C. A. Howard, D. J. L. Brett, P. R. Shearing, Z. Guo, I. P. Parkin, F. Li, *Nat. Energy* **2020**, *5*, 160.
[17] a) I. Harmanli, N. V. Tarakina, M. Antonietti, M. Oschatz, *J. Am. Chem. Soc.* **2021**, *143*, 9377; b) B. Kokoszka, N. K. Jarrah, C. Liu, D. T. Moore, K. Landskron, *Angew. Chem., Int. Ed.* **2014**, *53*, 3698.
[18] a) X. Tan, L. Kou, H. A. Tahini, S. C. Smith, *Sci. Rep.* **2015**, *5*, 17636; b) J. Yue, J. Zhang, Y. Tong, M. Chen, L. Liu, L. Jiang, T. Lv, Y. S. Hu, H. Li, X. Huang, L. Gu, G. Feng, K. Xu, L. Suo, L. Chen, *Nat. Chem.* **2021**, *13*, 1061.
[19] F. Weinhold, R. A. Klein, *Angew. Chem., Int. Ed.* **2014**, *53*, 11214.

[20] a) J. Avila, L. F. Lepre, C. C. Santini, M. Tiano, S. Denis-Quanquin, K. C. Szeto, A. A. H. Padua, M. C. Gomes, *Angew. Chem., Int. Ed.* **2021**, *60*, 12876; b) L. F. Lepre, M. C. Gomes, R. A. Ando, *ChemPhysChem* **2020**, *21*, 1230.
[21] S. Ringe, E. L. Clark, J. Resasco, A. Walton, B. Seger, A. T. Bell, K. Chan, *Energy Environ. Sci.* **2019**, *12*, 3001.
[22] M. Thommes, K. Kaneko, A. V. Neimark, J. P. Olivier, F. Rodriguez-Reinoso, J. Rouquerol, K. S. W. Sing, *Pure Appl. Chem.* **2015**, *87*, 1051.
[23] a) Q. Huang, Q. Luo, Y. Wang, E. Pentzer, B. Gurkan, *Ind. Eng. Chem. Res.* **2019**, *58*, 10503; b) N. Wu, X. Ji, W. Xie, C. Liu, X. Feng, X. Lu, *Langmuir* **2017**, *33*, 11719.
[24] M. Oschatz, M. Antonietti, *Energy Environ. Sci.* **2018**, *11*, 57.
[25] Z. Xiong, P. Guo, Y. Yang, S. Yuan, N. Shang, C. Wang, Y. Zhang, H. Wang, Y. Gao, *Adv. Energy Mater.* **2022**, *12*, 2103226.
[26] S. Liu, H. Yang, X. Huang, L. Liu, W. Cai, J. Gao, X. Li, T. Zhang, Y. Huang, B. Liu, *Adv. Funct. Mater.* **2018**, *28*, 1800499.
[27] L. Köps, F. A. Kreth, D. Leistenschneider, K. Schutjajew, R. Gläßner, M. Oschatz, A. Balducci, *Adv. Energy Mater.* **2023**, *13*, 2203821.
[28] S. Boyd, K. Ganeshan, W. Tsai, T. Wu, S. Saeed, D. Jiang, N. Balke, A. C. T. van Duin, V. Augustyn, *Nat. Mater.* **2021**, *20*, 1689.
[29] W. Chen, J. Gu, Q. Liu, M. Yang, C. Zhan, X. Zang, T. A. Pham, G. Liu, W. Zhang, D. Zhang, B. Dunn, Y. M. Wang, *Nat. Nanotechnol.* **2022**, *17*, 153.
[30] a) M. Chen, J. Wu, T. Ye, J. Ye, C. Zhao, S. Bi, J. Yan, B. Mao, G. Feng, *Nat. Commun.* **2020**, *11*, 5809; b) S. Bi, R. Wang, S. Liu, J. Yan, B. Mao, A. A. Kornyshev, G. Feng, *Nat. Commun.* **2018**, *9*, 5222.
[31] S. Azmi, M. F. Koudahi, E. Frackowiak, *Energy Environ. Sci.* **2022**, *15*, 1156.
[32] Y. Avni, R. M. Adar, D. Andelman, *Phys Rev E* **2020**, *101*, 010601.
[33] M. Sevilla, P. Valle-Vigón, A. B. Fuertes, *Adv. Funct. Mater.* **2011**, *21*, 2781.
[34] C. Cadena, J. L. Anthony, J. K. Shah, T. I. Morrow, J. F. Brennecke, E. J. Maginn, *J. Am. Chem. Soc.* **2004**, *126*, 5300.
[35] J. P. de Souza, Z. A. H. Goodwin, M. McEldrew, A. A. Kornyshev, M. Z. Bazant, *Phys. Rev. Lett.* **2020**, *125*, 116001.
[36] Z. Huang, T. Wang, X. Li, H. Cui, G. Liang, Q. Yang, Z. Chen, A. Chen, Y. Guo, J. Fan, C. Zhi, *Adv. Mater.* **2022**, *34*, 2106180.
[37] S. Zeng, X. Zhang, L. Bai, X. Zhang, H. Wang, J. Wang, D. Bao, M. Li, X. Liu, S. Zhang, *Chem. Rev.* **2017**, *117*, 9625.
[38] Y. Liu, B. Soucaze-Guillous, P.-L. Taberna, P. Simon, *J. Power Sources* **2017**, *366*, 123.
[39] a) H. Zhao, H. Zhang, Z. Wang, X. Jiang, Y. Xie, Z. Xu, Y. Wang, W. Yang, *ChemSusChem* **2021**, *14*, 3895; b) H. A. Andreas, *J. Electrochem. Soc.* **2015**, *162*, A5047.
[40] a) E. Mourad, L. Coustan, P. Lannelongue, D. Zigah, A. Mehdi, A. Vioux, S. A. Freunberger, F. Favier, O. Fontaine, *Nat. Mater.* **2017**, *16*, 446; b) M. Xia, J. Nie, Z. Zhang, X. Lu, Z. L. Wang, *Nano Energy* **2018**, *47*, 43.
[41] X. Li, T. Guo, L. Zhu, C. Ling, Q. Xue, W. Xing, *Chem. Eng. J.* **2018**, *338*, 92.
[42] W. Guo, F. Yang, C. Yu, Y. Xie, J. Chen, Y. Liu, Y. Zhao, J. Yang, X. Feng, S. Li, Z. Wang, J. Yu, K. Liu, K. Qian, M. Tsige, Q. Zhang, J. Guo, J. Qiu, *Matter* **2021**, *4*, 2902.
[43] W. Guo, C. Yu, S. Li, J. Qiu, *Energy Environ. Sci.* **2021**, *14*, 576.
[44] S. Leyva-García, D. Lozano-Castelló, E. Morallón, T. Vogl, C. Schütter, S. Passerini, A. Balducci, D. Cazorla-Amorós, *J. Power Sources* **2016**, *336*, 419.
[45] a) M. Shi, P. Xiao, J. Lang, C. Yan, X. Yan, *Adv. Sci.* **2020**, *7*, 1901975; b) Z. Gan, Y. Wang, M. Wang, E. Gao, F. Huo, W. Ding, H. He, S. Zhang, *J. Mater. Chem. A* **2021**, *9*, 15985.
[46] S. Xu, S. Xing, S. Pei, V. Ivanistsev, R. Lynden-Bell, S. Baldelli, *J Phys Chem* **2015**, *119*, 26009.
[47] J. Xiao, X. Zhang, H. Fan, Q. Lin, L. Pan, H. Liu, Y. Su, X. Li, Y. Su, S. Ren, Y. Lin, Y. Zhang, *Adv. Energy Mater.* **2022**, *12*, 2202602.
[48] A. A. Lee, C. S. Perez-Martinez, A. M. Smith, S. Perkin, *Phys. Rev. Lett.* **2017**, *119*, 026002.
[49] M. A. Gebbie, H. A. Dobbs, M. Valtiner, J. N. Israelachvili, *Proc Natl Acad Sci U S A* **2015**, *112*, 7432.
[50] A. M. Smith, A. A. Lee, S. Perkin, *J. Phys. Chem. Lett.* **2016**, *7*, 2157.
[51] C. Prehal, C. Koczwara, H. Amenitsch, V. Presser, O. Paris, *Nat. Commun.* **2018**, *9*, 4145.
[52] a) J. W. To, J. He, J. Mei, R. Haghpanah, Z. Chen, T. Kurosawa, S. Chen, W. G. Bae, L. Pan, J. B. Tok, J. Wilcox, Z. Bao, *J. Am. Chem. Soc.* **2016**, *138*, 1001; b) J. Gong, M. Antonietti, J. Yuan, *Angew. Chem., Int. Ed.* **2017**, *56*, 7557.
[53] N. Dubouis, P. Lemaire, B. Mirvaux, E. Salager, M. Deschamps, A. Grimaud, *Energy Environ. Sci.* **2018**, *11*, 3491.
[54] H. Zhang, Y. Zhong, J. Li, Y. Liao, J. Zeng, Y. Shen, L. Yuan, Z. Li, Y. Huang, *Adv. Energy Mater.* **2022**, *13*, 2203254.
[55] X. Wang, L. Lu, B. Wang, Z. Xu, Z. Xin, S. Yan, Z. Geng, Z. Zou, *Adv. Funct. Mater.* **2018**, *28*, 1804191.
[56] J. Le, Q. Fan, J. Li, J. Cheng, *Sci. Adv.* **2020**, *6*, eabb1219.
[57] F. Coupette, A. A. Lee, A. Hartel, *Phys. Rev. Lett.* **2018**, *121*, 075501.
[58] a) J. Zhao, Y. Jiang, H. Fan, M. Liu, O. Zhuo, X. Wang, Q. Wu, L. Yang, Y. Ma, Z. Hu, *Adv. Mater.* **2017**, *29*, 1604569; b) V. Sedajova, A. Bakandritsos, P. Blonski, M. Medved, R. Langer, D. Zaoralova, J. Ugolotti, J. Dzibelova, P. Jakubec, V. Kupka, M. Otyepka, *Energy Environ. Sci.* **2022**, *15*, 740.